Available online at www.sciencedirect.com
SCIENCE DIRECT®

Journal of the European Ceramic Society 24 (2004) 2293–2301
www.elsevier.com/locate/jeurceramsoc

Improvement in the thermal shock resistance of alumina through the addition of submicron-sized aluminium nitride particles

María Isabel Nieto[a], Rafael Martínez[a], Leo Mazerolles[b], Carmen Baudín[a,*]

[a]*Instituto de Cerámica y Vidrio, CSIC Campus de Cantoblanco, 28049 Madrid, Spain*
[b]*Centre d'Etudes de Chimie Metallurgique, CNRS UPR 2801, 94407 Vitry Cedex, France*

Received 1 April 2003; received in revised form 23 July 2003; accepted 29 July 2003

Abstract

The possibility of improving the thermal shock behaviour of alumina under mild thermal conditions due to the addition of submicron-sized and homogeneously dispersed AlN particles is studied. Processing conditions were adjusted in order to avoid the formation of AlON and, consequently, a decrease in the thermal conductivity of the composite. To evaluate the thermal shock behaviour, samples containing Vickers indentations were tested in quenching and the growth of the radial cracks was determined. Glycerine was chosen as the quenching fluid to minimize the effect of boiling on the heat transfer coefficient and to assure mild heat transfer conditions. A reference alumina material and a composite alumina + 10 vol% AlN with similar microstructural characteristics were prepared. The materials properties controlling the thermal shock response of the materials, i.e. Young's modulus, fracture toughness, coefficient of thermal expansion and thermal conductivity were determined and the theoretical relationships for the growth of the cracks were calculated and compared with the experimental results. The combination of thermal and mechanical properties of the composite leads to an improvement in the thermal shock resistance of alumina in terms of critical temperature increment ($\cong 50\%$) which is in agreement with the value predicted by theory.

Keywords: Al_2O_3-AlN composite; Thermal conductivity; Thermal expansion; Thermal shock resistance; Toughness; Young's modulus

1. Introduction

Monophase dense alumina materials are well known for their advantageous properties, such as wear and deformation resistance and chemical inertness, but they lack thermal shock resistance.

The thermal stresses developed in a piece of elastic material subjected to a sudden temperature change are proportional to the product of the thermal expansion coefficient, α, and the Young's modulus, E, of the material. As a consequence, the classical parameter, R, that describes the thermal shock resistance of brittle materials in terms of the maximum temperature increment that the material can stand without fracture is given by[1]:

$$R = \frac{\sigma_f}{E \cdot \alpha} \cdot (1 - \nu) \quad (1)$$

where σ_f, E, ν and α are the strength, the Young's modulus, the Poisson's coefficient and the coefficient of thermal expansion of the material.

Under mild thermal shock conditions, the response of the material is determined also by its thermal conductivity, k, and the classical parameter R' is given by:

$$R' = k \cdot \frac{\sigma_f}{E \cdot \alpha} \cdot (1 - \nu) \quad (2)$$

In monophase dense ceramics it is difficult to increase this parameter because α is almost fixed by phase composition and the potential ways to decrease E, e.g., increase porosity or microcrack density, are usually accompanied by a decrease in strength and thermal conductivity.

Two phase materials will present better thermal shock resistance than the matrix, in terms of the maximum temperature increment that the material can stand without fracture, ΔT_c, if the second phase has lower product E·α and/or higher thermal conductivity than the matrix. Strength values can be maintained in the

* Corresponding author. Tel.: +34-91-735-5843; fax: +34-91-735-5843.
E-mail address: cbaudin@icv.csic.es (C. Baudín).

0955-2219/$ - see front matter © 2003 Elsevier Ltd. All rights reserved.
doi:10.1016/j.jeurceramsoc.2003.07.011

composite by means of a strict microstructural control, or even increased due to the toughening effect of the second phase.

In previous works,[2,3] we have used this approach to develop alumina–mullite and alumina–aluminium titanate composites with improved thermal shock response. The level of improvement in terms of ΔT_c agreed qualitatively with theoretical predictions. For an alumina–10 vol% mullite material,[2] the increase in the critical temperature increment (≈12%) was due solely to the decrease of the product $E{\cdot}\alpha$, whereas for a composition alumina–10 vol% aluminium titanate,[3] ΔT_c was further increased (≈30–40%) due to the toughening effect of the second phase. Moreover, the hardness and strength of alumina were maintained in these composites.

Using a similar approach, alumina–metal[4–7] and alumina–tungsten carbide[8] composites with improved thermal shock resistance under severe thermal shock conditions, i.e. quenching in water at room temperature were also developed. Critical temperature increments higher than those of alumina were reported for alumina–molybdenum (20 vol%),[6] alumina–iron (20 vol%),[4,5] alumina–copper (5 vol%)[7] and alumina–tungsten carbide[8] composites, and related to the reduction in Young's modulus and the increase in thermal conductivity[4–7] and the increase in toughness.[7,8]

Aluminium nitride is another possible ceramic second phase to improve the thermal shock resistance of alumina. There is not general agreement about the compatibility of AlN and alumina.[9–12] In particular, there is uncertainty about the formation of AlON as a function of temperature and atmosphere, due to the fact that stability in this system is highly dependent on oxygen and nitrogen partial pressures and both are determined by the gas flow rate and the furnace design, i.e. the presence of graphite. Moreover, the physical characteristics of the powders will determine the microstructural evolution during the low temperature treatments and, consequently, the accessibility of the atmospheric gas to the bulk of the compacts at higher temperature. Lastly, differences in the chemical composition of the powders, in particular the nature and amount of impurities, will also determine the phase equilibrium relationships.

Using thermodynamic data, Willems et al.[12] showed that AlON is stable only within a small region of oxygen and nitrogen pressures and that it is not stable below 1640 ± 10 °C. Even though, several authors have found AlON at temperatures as low as 1600 °C,[13] most experiments, performed in graphite furnaces and under flowing N_2, indicate that the stable phases below 1700 °C are AlN and Al_2O_3, while γ-AlON appears first at 1700 °C.[9–11]

Reported values of Young's modulus (350 GPa at 25 °C)[14,15] and coefficient of thermal expansion ($\alpha_{25-1000\ ^\circ C} = 5.6\text{-}5.7\times10^{-6}{}^\circ C^{-1}$)[14] for high purity and dense AlN materials are lower than those of dense alumina[3] ($E = 405\pm2$ GPa at 25 °C, and $\alpha_{25-600\ ^\circ C} = 9.4\pm0.2\times10^{-6}{}^\circ C^{-1}$). For aluminium oxynitride spinel materials, stiffness is lower ($E = 307$–330 GPa,[16,17] at 25 °C), and thermal expansion is slightly higher ($\alpha_{20-1000\ ^\circ C}\approx7.0\text{–}7.4\times10^{-6}{}^\circ C^{-1}$)[18] than for aluminium nitride.

For pure AlN single crystal, theoretical thermal conductivity along the *c*-axis was predicted to be 319 W/mK.[19] While values as high as 285 W/mK have been reported for very pure single crystals,[19] substantial variability (≈70–260 W/mK at 25 °C) exists for polycrystalline dense AlN materials depending on composition, i.e. second phases and oxygen content, and microstructure.[14,20–26] The thermal conductivity of aluminium oxynitride spinels is much lower (≈9–11 W/mK[18,27] at 25 °C), and in the same range of that of the highly conductive oxides.

Even though the product E·α for AlN and AlON is lower than that for alumina, the reported thermal shock behaviour of hot pressed AlN and AlON ceramics under severe thermal conditions (25 °C water quench test) was similar to that of alumina,[15,18] which can be attributed to the relatively poor mechanical properties of the materials tested ($K_{IC}\approx2\text{–}3$ MPam$^{1/2}$, $\sigma_f\approx200\text{–}350$ MPa) compared with those for similarly processed aluminas ($K_{IC}\approx3\text{–}4$ MPam$^{1/2}$, $\sigma_f\approx400\text{–}500$ MPa).[28,29] However, the thermal shock behaviour of AlN under mild thermal conditions, where the beneficial effect of the higher thermal conductivity is expected, should be much better than that of alumina, as described by R' [Eq. (2)].

In this work, the possibility of improving the thermal shock behaviour of alumina under mild thermal conditions by the addition of submicron-sized and homogeneously dispersed AlN particles is studied. Processing conditions were adjusted in order to avoid the formation of AlON and, consequently, the decrease in the thermal conductivity of the composite. In principle, two different factors might play a role in the thermal response of the composite. First, from the above mentioned data, the product $E{\cdot}\alpha$ for AlN (≈1.7 MPa°C^{-1}) is about half of that for alumina (≈3.8 MPa°C^{-1}). Second, the dispersion of a highly conductive phase would improve the thermal conductivity of the alumina matrix, as observed for vacuum sintered cordierite (92–66 vol%)–AlN (8–34 vol%) composites.[30] Moreover, AlN might have some toughening effect on the composite due to its thermal expansion mismatch with alumina, as observed for alumina–aluminium titanate.[3]

Thermal shock test

In order to reduce the statistical effects associated to the quenching-strength method, indented samples have been successfully used by different authors to evaluate the relative thermal shock resistance of a number of dense ceramics.[2,3,31–37] In this work, Vickers indented

samples were tested in quenching and the growth of the radial cracks as a function of the severity of the thermal shock was analyzed to evaluate the thermal shock behaviour. A modification of the method initially proposed by Osterstock et al.[33,34] to analyze the evolution of cracks with different sizes under the same thermal shock conditions, i.e. temperature increment, ΔT, was used in order to evaluate the thermal shock resistance of the materials in terms of the applied temperature increment.[2,3] Even though this simplified analysis does not consider the existent differences between the thermal states of the surface and the bulk of the specimens,[32,35] it describes essentially the crack growth versus temperature increment curve and accounts for the effect of the materials properties on the thermal shock response.

The analysis of the symmetric crack pattern that appears at the corners of the Vickers indentations in brittle materials[38–40] shows that the stress intensity factor, K_0 at the tip of a Vickers indentation flaw of length, C_0, formed due to the effect of a load, P, is given by:

$$K_0 = K_c = \chi_r \cdot P \cdot C_0^{-3/2} \tag{3}$$

where K_C is the fracture toughness of the material and χ_r is known as the residual stress factor and is a function of the Young's modulus and the hardness of the material and the geometry of the contact between the indenter and the surface of the material.

When a specimen containing a Vickers indentation performed at a load P is quenched, a surface thermal stress, σ_T, dependent on the temperature difference of the thermal shock, ΔT, is produced. Therefore, the residual stress associated with the indentation is supplemented by the additional stress, σ_T. For the indentation crack to advance under equilibrium conditions, the total stress intensity factor has to be equal to the fracture toughness of the material, K_C, and the following relation between the thermal stress and the crack size is obtained:[34,35]

$$\sigma_T = \frac{K_c}{(\Omega \cdot \pi \cdot C)^{1/2}} \cdot \left(1 - \frac{\lambda \cdot \chi_r \cdot P}{K_c \cdot C^{3/2}}\right) \tag{4}$$

where $(\Omega\pi C)^{1/2}$ is a geometrical factor for the stress intensity field of a half penny surface crack and λ ($0 \leqslant \lambda \leqslant 1$) describes the extent of relief of residual indentation stress resulting from the heating/quenching operation.

Taking into account Eq. (3), the thermal stress can be expressed in terms of the initial crack length C_0:

$$\sigma_T = \chi_r \cdot P \cdot \left(C_0^{-3/2} - \lambda \cdot C^{-3/2}\right)/(\Omega \cdot \pi \cdot C)^{1/2} \tag{5}$$

The initial indentation crack of size C_0 experiences stable crack growth, under the applied thermal stress up to a critical size C_c[33,34]:

$$C_c = \left(\frac{4 \cdot \lambda \cdot \chi_r \cdot P}{K_c}\right)^{2/3} \tag{6}$$

The associated stress value when $C = C_c$ is:

$$\sigma_c = 0.47 \cdot K_c^{4/3}/(\pi \cdot \Omega)^{1/2} \cdot (\lambda \cdot \chi_r P)^{1/3} \tag{7}$$

On this basis, Osterstock et al.[33,34] proposed and tested an experimental method to evaluate the relative performance of materials submitted to thermal shock. The samples were indented using different indentation loads, P, and subjected to a fixed temperature increment, ΔT. The curves of relative increase of crack length, C/C_0, vs indentation load reflected the empirical ranking of thermal shock resistance of the materials tested.

In this work, a different procedure was used[2,3] in order to compare the materials in terms of the critical temperature increment. If different samples of a material are indented with the same load and subjected to increasing temperature increments, ΔT, the pattern of crack growth is divided into three regimes: At low ΔT, no significant crack growth can be detected; in a medium ΔT interval the crack growth is stable; and from a larger ΔT value, the crack grows unstably.[2,3,35]

For increasing temperature increments, under mild and constant heat transfer conditions and convection being the main heat transfer mechanism, the thermal stress will increase according to:[1,41]

$$\sigma_T = E \cdot \alpha \cdot \Delta T \cdot \frac{f(\beta)}{(1-\nu)} \tag{8}$$

where E, α and ν are the Young's modulus, the thermal expansion coefficient and the Poisson's coefficient of the material. $f(\beta)$ stands for geometry and heat transfer conditions and is a function of the Biot modulus,[41] $\beta = ah/k$, with h being the surface heat transfer coefficient, k the thermal conductivity of the material and a the characteristic heat transfer length.

From Eqs. (5) and (8):

$$\Delta T = \chi_r \cdot P \cdot \left(C_0^{-3/2} - \lambda \cdot C^{-3/2}\right)/(\Omega \cdot \pi \cdot C)^{1/2} \cdot \frac{(1-\nu)}{E \cdot \alpha} \cdot \frac{1}{f(\beta)} \tag{9}$$

The theoretical relationships derived from Eq. (9) for the monophase alumina and the composite have been calculated and compared to the experimental thermal shock results for the evolution of indentation cracks of equal initial crack length with increasing ΔT.

Water at room temperature is one of the fluids most used as quenching medium in thermal shock tests. Nevertheless, this medium presents serious problems when used to test alumina-based dense materials, as they usually fail when cooled from temperatures around 200–300 °C. Samples at these temperatures originate the

boiling of the water when they enter in contact with it, and, as a consequence, the surface heat transfer coefficient, h, experiences large variations, up to 2–3 orders of magnitude, for $\Delta T = 200$–300 °C.[42]

To minimize the effect of boiling on the heat transfer coefficient and, consequently, its variability in the range of testing temperatures, glycerine was chosen as quenching fluid due to its relatively high ebullition point (≈290 °C).[43] Moreover, the high viscosity (≈900 mPa·s)[43] and relatively low thermal conductivity (≈0.3 W/m°C)[43] of this medium assured mild heat transfer conditions to account for the effect of AlN on the thermal conductivity of alumina.

2. Experimental

Commercial Al_2O_3 (Condea HPA05, Germany) and AlN (ACST, grade B, Germany) were used as starting powders, with a mean particle size (laser diffraction, Malvern Mastersizer S, UK) of 0.4 μm for alumina and 2.1 μm for aluminium nitride and a specific surface area (N_2 adsorption, BET, Monosorb, Quantachrome, USA) of 9.5 and 5.3 m^2/g, for alumina and aluminium nitride, respectively. In order to decrease the AlN particle size, the powder was attrition milled with alumina balls for 10 h, to reach particle sizes smaller than 500 nm and a specific surface area of 14.8 m^2/g. The mixture Al_2O_3–10 vol% AlN (A10AlN) was attrition milled in isopropyl alcohol with alumina balls for 1 h, dried and sieved (63 μm).

The alumina + 10 vol%AlN mixture was hot pressed at 1550 °C and 40 MPa, for 30 min in a nitrogen atmosphere. Green compacts of alumina were obtained by isostatic pressing at 200 MPa and sintering was performed in an electric furnace at 1500 °C for 1 h. The monophase alumina thermal treatment was adjusted to obtain similar grains sizes as those of the alumina grains in the composite. The obtained materials will be denoted as A_M and A–10AlN, for the reference alumina and the composite, respectively.

The crystalline phases in the sintered composite were analysed by X-ray diffraction (Siemens, D-5000, Germany) using the files ASTM10-173 and 24-1133, for alumina and aluminium nitride, respectively.

Microstructural characterisation was by scanning electron microscopy (SEM, Zeiss DSM40, Germany) on fracture surfaces and on polished and thermally etched (1450 °C-1 h in a graphite furnace in flowing Nitrogen) surfaces, as well as by transmission electron microscopy (TEM, Jeol 2000FX, Japan). For TEM studies, specimens were thinned by mechanical polishing, dimpling and ion milling; images were obtained at 200 kV.

The average coefficient of thermal expansion between room temperature and 600 °C was determined in a Linear Voltage Displacement Transducer dilatometer (Adhamel Lomargy, France) with a quartz rod. Three samples of 12 mm length and 4×5 mm^2 cross section were diamond cut from the sintered blocks and tested for each material. Given values are the average of the three measurements and errors relate to the maximum and minimum obtained values.

Thermal diffusivity was determined from room temperature up to 400 °C in a laser flash equipment (Holometrix Thermal Flash, USA), using thin discs (diameter = 12.7 mm, thickness = 1 mm) diamond drilled and cut from the blocks. The specific heat was evaluated by comparison with a standard of alumina. Thermal conductivity, k, was calculated from these data and the density of the materials, determined by the Archimedes' method using water. Reported values for thermal conductivity are the average of three determinations and errors relate to the maximum and minimum obtained values.

Young's modulus of the reference alumina was determined by the resonance frequency method on parallelepiped bars (4×5×50 mm^3), diamond cut from the sintered blocks, tested in flexure, using a commercial apparatus (Lemmens Grindosonic MK5 Industrial, Belgium). Given values are the average of five bars, and errors are the standard deviation of the measurements. For the composite, Young's modulus was calculated using Voight equation:

$$E_c = v_A \cdot E_A + v_{AlN} \cdot E_{AlN} \quad (10)$$

where v_A and v_{AlN} are the volumetric fractions of alumina and AlN, respectively, and E_A and E_{AlN} are the Young's modulus of alumina and AlN, respectively. For E_A, the experimental value for the reference alumina (Table 1) and for AlN the experimental value reported for dense AlN materials (350 GPa)[14,15] were used.

Hardness, HV, and toughness, K_C, were determined from Vickers indentation tests (Leco Hardness Tester, Japan) on polished surfaces (1 μm), with indentation loads of 98 N during times of 10 s. No chipping associated with any indentation was detected and the indentations that exhibited secondary radial cracking were rejected. The principal diagonals of the plastically deformed zone and the length of the radial cracks were measured using a reflected light optical microscope (RLOM, Carl-Zeiss D-7082, Germany) to calculate HV and K_c values, respectively. The equation proposed by Miranzo and Moya[44] was used to calculate the constant χ_r [Eq. (3)] and K_c. Reported values are the average of ten determinations and errors are the standard deviations.

To fabricate small discs (diameter = 11.9, thickness = 3 mm) to be the thermal shock samples, cylinders were diamond drilled and embedded in a resin. One of the flat faces of the cylinder was diamond polished, down to 1 μm, and subsequently a slice of 3 mm width was cut from the cylinder with a fine diamond disc to obtain the

Table 1
Density and thermo-mechanical properties of the reference alumina and the composite A10AlN (alumina + 10 vol% AlN)

	Alumina	A-AlN
Density (g/cm^3)	3.94±0.02	3.90±0.01
% of theoretical	98.6	99.5
$\alpha_{200-600\ ^\circ C}$ ($\times 10^{-6}K^{-1}$)	9.4±0.2	9.1±0.2
Young's modulus (GPa)	405±2	373
Vicker's Hardness (GPa)	19.4±0.3	17.9±0.2
Toughness, Kc (MPam$^{1/2}$)	3.8±0.2	4.5±0.1

test sample. During the cutting process parallelism of the surfaces was maintained and dimensions were carefully checked. Previous to the thermal shock test, a Vickers indentation (98 N for 10 s) was introduced in the centre of the polished face of the discs. The indentations formed cracks of similar sizes in both materials ($C_0 = 203 \pm 10$ and 183 ± 8 μm for A_M and A–10AlN, respectively). For the thermal shock tests, each sample was fixed in an aluminium sample holder with open bottom. To avoid stress concentration at the edges and at the contact between the holder and the indented area of the specimen, a fibre blanket was placed around the lateral surface of the disc and extended 1 mm into the indented surface.

The holder was heated in a vertical electrical furnace using 5 °C/min as the heating rate and 20 min as the stabilisation time before quenching in a glycerine bath at 40 °C. The indented faces of the discs were placed facing the bottom of the holder and thus were the first to contact the cooling medium. The size of the indentation cracks was measured before and after the thermal shock test using a reflected light optical microscope (Carl-Zeiss D-7082, Germany).

3. Results and discussion

3.1. Microstructure and physical properties

In the composite material, only Al_2O_3 and AlN were identified by XRD, and no evidence of AlON was detected, as expected from the sintering schedule used ($T < 1640$ °C), in agreement with the thermodynamic data supplied by Willems et al.[12] and the phase equilibrium diagram proposed by McCauley and Corbin[10,11]

Table 1 summarises the densities and the thermo-mechanical properties of both materials and Figs. 1 and 2 show the microstructure of the composite. Aluminium nitride could not be differentiated from alumina by SEM of the polished surfaces (Fig. 1a); in these micrographs equi-dimensional grains of sizes between 0.5 and 3 μm were observed (Fig. 1a). Conversely, in the fracture surfaces (Fig. 1b) small (< 500 nm) and whiter grains were found located at triple points and inside the alumina grains. These small grains were identified by electron diffraction in the selected area diffraction mode (TEM) as aluminium nitride (Fig. 2). Both diffraction patterns accompanying images in Fig. 2 correspond to the (0001) plane of the AlN hexagonal structure ($a = 0.3111$ nm, $c = 0.4979$ nm, JCPDS 25–1133). The intra-granular AlN particles (< 200 nm, Fig. 2a) were smaller than those located at triple points and at grain boundaries (200–500 nm, Figs. 1 and 2b). Only alumina and aluminium nitride were observed by TEM, in agreement with the XRD results.

The contribution of AlN to the thermal expansion of the composite can be evaluated using the Turner's expression:[45]

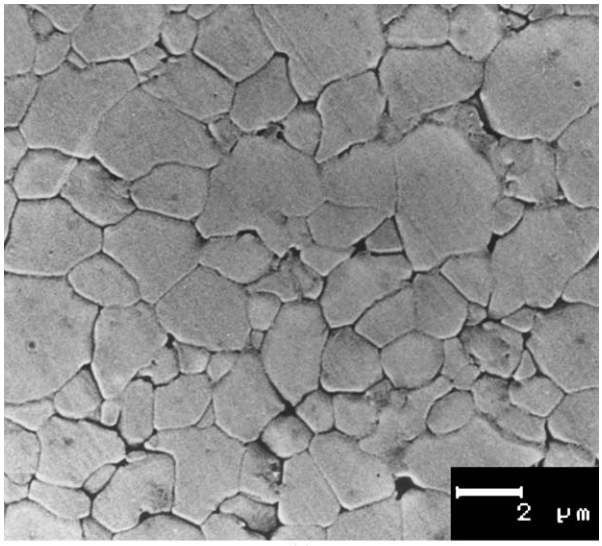

(a)

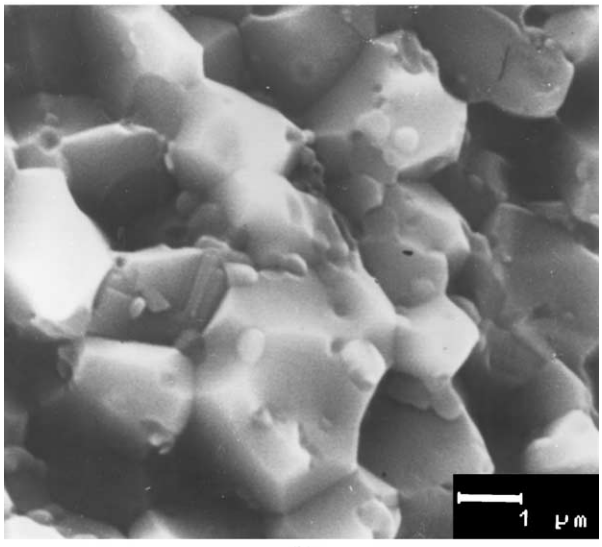

(b)

Fig. 1. Microstructure of the A10AlN (Alumina + 10 vol%AlN) composite. (a) SEM of a polished and thermally etched surface. Equi-dimensional grains of sizes between 0.5 and 3 μm are observed. (b) SEM of a fracture surface. Small (< 500 nm) and whiter grains are found located at triple points, grain boundaries and inside the alumina grains.

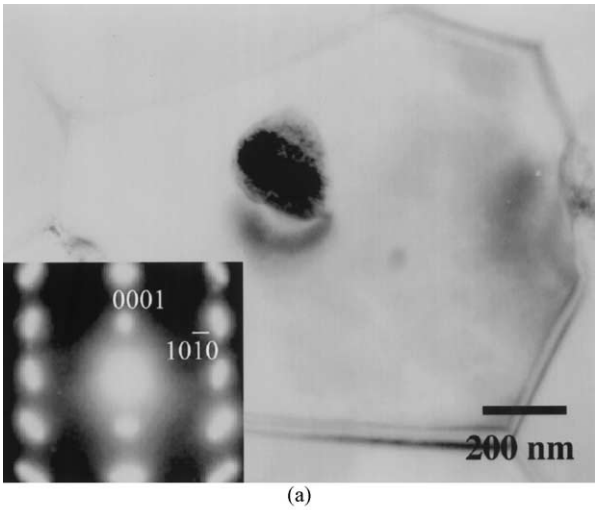

(a)

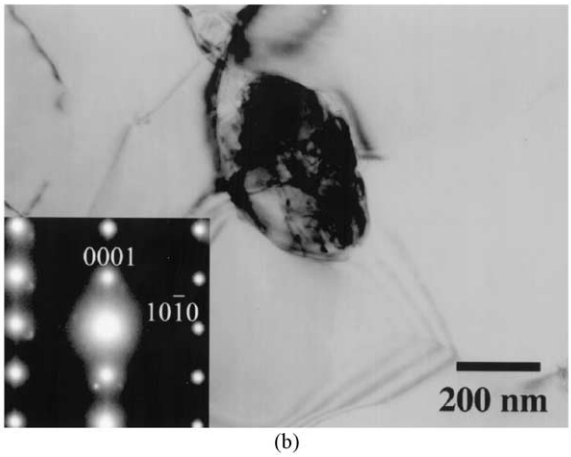

(b)

Fig. 2. TEM micrographs of the A10AlN composite. The two locations of the AlN particles are observed, as shown by the diffraction diagrams. (a) AlN particle embedded in an alumina grain. (b) AlN particle embedded located at a triple point.

$$\alpha_c = \frac{\dfrac{\alpha_A \cdot K_A \cdot v_A}{\rho_A}}{\dfrac{K_A \cdot v_A}{\rho_A}} + \frac{\dfrac{\alpha_{AlN} \cdot K_{AlN} \cdot v_{AlN}}{\rho_{AlN}}}{\dfrac{K_{AlN} \cdot v_{AlN}}{\rho_{AlN}}} \tag{11}$$

where α_c is the thermal expansion coefficient of the composite (Table 1), and α, ρ, v and K are the thermal expansion coefficient, the density, the volume fraction and the bulk modulus of alumina (A) and aluminum nitride (AlN), respectively.

The bulk modulus of the material, K, is given by:

$$K = \frac{E}{3 \cdot (1 - 2 \cdot \upsilon)} \tag{12}$$

where E is the Young's modulus and v is the Poisson coefficient of the material.

Introducing the values of the properties summarised in Table 1, and assuming coincident values of the Poisson coefficient for both materials, a value of $5.8 \times 10^{-6} {}^{\circ}C^{-1}$ is obtained for the thermal expansion coefficient of the AlN particles dispersed in the alumina matrix. This value is coincident with that reported for high purity and dense aluminium nitride ceramics.[14]

Hardness of the composite (Table 1) is slightly lower than that of alumina, as expected due to the addition of second phase with lower hardness (H≈14–15 GPa for dense AlN[17,18]), but still in the range of the hardness of dense aluminas. This value is coincident with that reported for hot pressed alumina–AlN composites with similar composition (≈18GPa).[14]

Toughness of the composite is higher than that of alumina, as reported for an alumina (90 vol%) + AlON (10 vol%) composite ($K_{IC} = 4.35$ MPam$^{1/2,}$ SENB).[29] Conversely, larger amounts (>20 vol%) of AlON were reported to have no effect[29] or even decrease[46] the toughness of the alumina matrix. The exact mechanism acting during fracture of the alumina–AlN composite studied here has to be further analysed but, in principle, microcracking and/or crack bridging might occur due to the compressive stresses developed around the second phase particles originated by the thermal expansion mismatch between alumina and AlN. The presence of radial microcracks around some AlN particles in the samples observed by TEM (Fig. 3) is evidence of these stresses.

Thermal conductivity as a function of temperature is plotted in Fig. 4. Values are higher for the composite across the whole temperature range tested. Room temperature value is significantly higher than the value (≈18 W/mK)[14] reported for alumina–AlN composites of similar composition hot pressed at 1700–1800 °C. This difference can be attributed to the presence of significant amounts of AlON in the latter materials due to the higher sintering temperatures.

The contribution of the AlN particles to the thermal conductivity of the composite, k_c, can be calculated by fitting the Maxwell relationship for composite materials:[45]

$$k_c = k_A \frac{1 + 2 \cdot v_{AlN} \cdot (1 - k_A/k_{AlN})/(2k_A/k_{AlN} + 1)}{1 - v_{AlN}(1 - k_A/k_{AlN})/(k_A/k_{AlN} + 1)} \tag{13}$$

Where k is the thermal conductivity, and v, A, and AlN stand for the volumetric fraction, alumina and aluminium nitride, as previously.

In order to eliminate the effect of porosity differences (Table 1) the thermal conductivity values for dense materials were calculated from the experimental values (Fig. 4) using the Klemens approximation:[47]

$$\frac{k\text{p(porous)}}{k\text{p(dense)}} = 1 - \frac{4}{3}\phi \tag{14}$$

Were, ϕ is the pore volume fraction.

Introducing room temperature values, a thermal conductivity value of about 50 W/mK is obtained for the

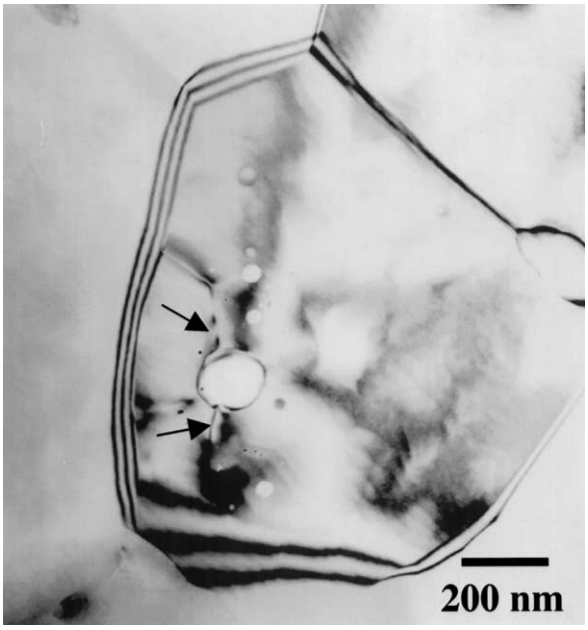

Fig. 3. TEM of the composite A10AlN material showing an intragranular AlN particle with associated radial microcracks signalled by arrows.

aluminium nitride particles, which is in the range of those (69.5 W/mK[22] and 62 W/mK[23] for AlN–Y_2O_3–Al_2O_3 sintered at 1850 and 1750 °C, respectively) reported for dense AlN materials with high oxygen contents in the AlN grains ($\geqslant$1.5 wt.%).

The evolution of thermal conductivity of the composite with temperature, plotted in Fig. 4, as well as the values of the coefficient of thermal expansion and hardness demonstrate that no or few microcracks are present in this material. Therefore, it is justified the use of the Voight expression [Eq. (10)] to calculate the Young's modulus of this material. The microcracks observed by TEM might be formed during the preparation process of the samples due to the high residual stresses present in the material.

3.2. Thermal shock

In Fig. 5 the experimental results for thermal shock are plotted. There is a threshold temperature increment for crack propagation, ΔT_0, for each material, $\Delta T_0 \approx 180$ °C for alumina and 300 °C $< \Delta T_0 <$ 400 °C for the composite. Collin and Rowcliffe observed this temperature threshold for a number of different materials quenched in water at room temperature, and concluded that it was due to the large differences between the heat transfer coefficients of surfaces at temperatures lower and higher than 100 °C.[35] This argument can not be applied to the experiments reported here in which the heat transfer coefficient is low and essentially constant across the whole range of temperature increments considered.

Taking into account Eq. (4), the existence of the threshold temperature might be due to stress relief ($\lambda < 1$). As no chipping was observed in any of the tested samples, no stress relief occurred by additional lateral cracking. Moreover, no stress relief by mass transport is expected during heating of alumina based materials due to the relatively low temperatures involved. Lee et al.[36] attributed the existence of this temperature threshold in indentation-quench tests of silicon nitride to post-indentation relaxation of residual contact stresses before quenching. On the other hand, the analysis by Fett[48] indicates that the action of a crack opening force, such as the thermal stress considered here, will also lead to the relaxation of the residual stresses.

Stable crack growth occurred in all samples tested using ΔT lower or equal to 300 and 500 °C for alumina

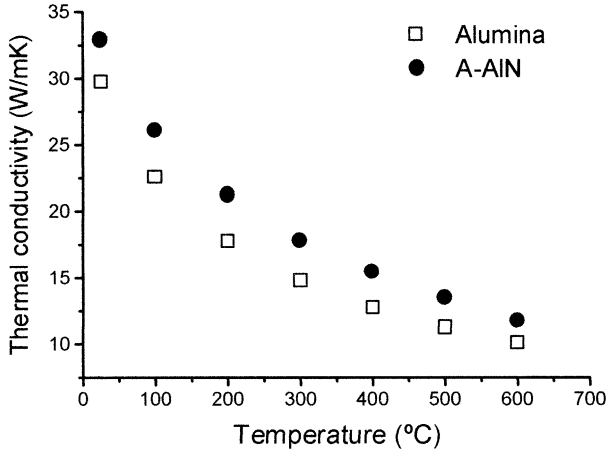

Fig. 4. Thermal conductivity as a function of temperature for the reference alumina material and the composite A10AlN (alumina + 10 vol% of AlN). The size of the symbols accounts for experimental variability.

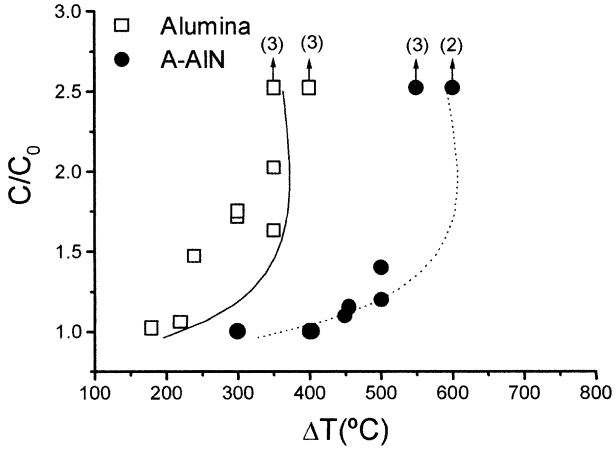

Fig. 5. Thermal shock test results for the reference alumina material and the composite A10AlN (alumina + 10 vol% of AlN). Relative crack growth (C/C_0) versus temperature increment. Lines corresponds to the theoretical relationships [Eq. (9)] calculated from the properties of the materials.

and A-10AlN, respectively ($C/C_0 \leqslant 1.7$, Fig. 5). The radial cracks traversed more than 50% of the samples tested for ΔT larger or equal to 350 and 550 °C for alumina and the composite, respectively. Therefore, the critical temperature increments, ΔT_C, are located between 300 and 350 °C for alumina and between 500 and 550 °C for A-10AlN, giving the following ratio between the critical temperature increments for the reference alumina, ΔT_C A and the composite, ΔT_C A–10AlN:

$$1.4 \leqslant \frac{\Delta T_{CA-10AlN}}{\Delta T_{CA}} < 1.8 \quad (15)$$

This level of improvement of the thermal shock of alumina in terms of ΔT_c is comparable to that found for alumina–iron (20 vol%)[5,6] and alumina–copper (5 vol%)[7] composites obtained by hot pressing for which the ratio was 1.5, and higher than those found for alumina–mullite[2] and alumina–aluminum titanate composites[3] tested under the same thermal conditions as those used here.

The value of λ can be estimated from the experimental results from Fig. 5. Taking into account Eqs. (3) and (6), the following relationship between the initial and the critical crack sizes and is obtained:

$$C_c = (4 \cdot \lambda)^{2/3} \cdot C_0 \quad (16)$$

From Eqs. (9) and (16) and making $\Delta T_0 = \Delta T$, for $C = C_0$ and $\Delta T_C = \Delta T$, for $C = C_C$:

$$\frac{\Delta T_0}{\Delta T_C} = 2.13 \cdot (1 - \lambda) \cdot \lambda^{-1/3} \quad (17)$$

Introducing the experimental values of ΔT_0 and ΔT_C for the reference alumina and the composite, $\lambda \approx 0.7$ is obtained for both materials, which indicates that a stress release of about 30% occurs. This value is in the range of those calculated from experimental data from other authors (0.6–0.7)[49,50] and for alumina–mullite and alumina–aluminium titanate composites tested under similar thermal conditions (≈0.7).[3,4] For this λ value, C_C/C_0 in Eq. (16) is about 2, in agreement with the fact that, relative crack lengths $C/C_0 \leqslant 1.7$ were determined in all samples in which stable fracture was observed.

The experimental values plotted in Fig. 5 can be compared with the theoretical relationships derived from Eq. (9). For Biot modulus lower than 5, the function $f(\beta)$ in Eqs. (8 and 9) can be approximated by:[41]

$$f(\beta) = \frac{\beta}{B} \quad (18)$$

where B is a constant between 3 and 4.

The Biot modulus for the experiments considered here, evaluated from the value of the heat transfer coefficient determined by Sato et al.[51] for quenching of tetragonal zirconia in glycerine (≈1000 W/m^{2}K), the size of the samples (3 mm) and the thermal conductivity values from Fig. 4, is $\beta < 1$, therefore, Eq. (18) can be applied.

In Fig. 5, the theoretical relationships derived from Eq. (9) and data from Table 1 and Fig. 4 are plotted. $B = 3.25$, as proposed by Manson,[41] $h = 1000$ W/m^{2}K,[51] and the thermal conductivity of the bulk of the samples ($T \approx 300$ °C) have been used to evaluate the Biot modulus for each material. From this plot, $\Delta T_C = 370$, 585 °C are derived for alumina and the composite, respectively, which ratio (1.58) is very close to the experimental one [Eq. (15)].

4. Conclusions

Small concentrations (10 vol%) of aluminium nitride added to alumina in the form of submicron sized and homogeneously distributed particles lead to a decrease in Young's modulus and thermal expansion coefficient of the alumina matrix and an increment in toughness. Thermal conductivity is increased when the presence of AlON phases is avoided by low temperature thermal treatment in a graphite furnace in flowing nitrogen. The combination of thermal and mechanical properties—thermal conductivity, thermal expansion coefficient, Young's modulus and toughness—of the composite leads to an improvement of the thermal shock resistance of alumina in terms of the critical temperature increment (≅50%) which agrees with that derived from theoretical calculations.

Acknowledgements

This work has been supported by CICYT (Spain, contract MAT2000-0949).

References

1. Hasselman, D. P. H., Thermal stress resistance parameters for brittle refractory ceramics: a compendium. *Am. Ceram. Soc. Bull.*, 1970, **49**(12), 1033–1037.
2. Mezquita, S., Uribe, R., Moreno, R. and Baudín, C., Influence of mullite additions on thermal shock resistance of dense alumina materials. part II: thermal properties and thermal shock behaviour. *Brit. Ceram. Trans.*, 2001, **100**(6), 246–250.
3. Uribe, R. and Baudín, C., Influence of a dispersion of aluminum titanate particles of controlled size on the thermal shock resistance of alumina. *J. Am. Ceram. Soc.*, 2003, **86**(5), 846–850.
4. Aldridge, M. and Yeomans, J. A., The thermal shock behaviour of ductile particle toughened alumina composites. *J. Eur. Ceram. Soc.*, 1998, **19**(9), 1769–1775.
5. Aldridge, M. and Yeomans, J. A., The thermal shock behavior of iron-particle-toughened alumina. *J. Am. Ceram. Soc.*, 2001, **84**(3), 603–607.
6. Sbaizero, O. and Pezzotti, G., Influence of molybdenum particles on thermal shock resistance of alumina matrix ceramics. *Mater. Sci. Eng.*, 2003, **A343**(1-2), 273–281.
7. Wang, L., Shi, J. L., Lin, M. T., Chen, H. R. and Yan, D. S., The thermal shock behavior of alumina-cooper composite. *Mater. Res. Bull.*, 2001, **36**(3-4), 932–952.

8. Wang, L., Shi, J.-L., Gao, J.-H. and Yan, D.-S., Influence of tungsten carbide particles on resistance of alumina matrix ceramics to thermal shock. *J. Eur. Ceram. Soc.*, 2001, **21**(9), 1213–1217.
9. Kim, N. H., Fun, Q. D., Komeya, K. and Meguro, T., Phase reaction and sintering behavior in the pseudoternary system AlN–Y_2O_3–Al_2O_3. *J. Am. Ceram. Soc.*, 1996, **79**(10), 2645–2651.
10. McCauley, J. W. and Corbin, N. D., High temperature reactions and microstructures in the Al_2O_3–AlN system. In *Progress in Nitrogen Ceramics*, ed. F. L. Riley. Martinus Nijhoff Publishers, The Hague (The Netherlands), 1983, pp. 111–118.
11. McCauley, J. W. and Corbin, N. D., Phase relations and reaction sintering of transparent cubic aluminum oxynitride spinel (ALON). *J. Am. Ceram. Soc.*, 1979, **62**(9–10), 476–479.
12. Willems, H. X., Hendrix, M. M. R. M., Metselaar, R. and de With, G., Thermodynamics of AlON I: stability at lower temperatures. *J. Eur. Ceram. Soc.*, 1992, **10**(2), 327–333.
13. Kim, Y. W., Park, H. C., Lee, Y. B., Oh, K. D. and Stevens, R., Reaction sintering microstructural development in the system Al_2O_3–AlN. *J. Eur. Ceram. Soc.*, 2001, **21**(13), 2383–2391.
14. Kieffer, R., Wruss, W. and Willer, B., Propriétés physiques et mécaniques de céramiques AlN–Al_2O_3 obtenues par compression à chaud. *Rev. Int. Htes. Temp. et Réfract.*, 1976, **13**(2), 97–107.
15. Boch, P., Glandus, J. C., Jarrige, J., Lecompte, J. P. and Mexmain, J., Sintering, oxidation and mechanical properties of hot pressed aluminum nitride. *Ceramics International*, 1982, **8**(1), 34–40.
16. Graham, E. K., Munly, W. C., McCauley, J. W. and Corbin, N. D., Elastic properties of polycrystalline aluminum oxynitride spinel and their dependence on pressure, temperature, and composition. *J. Am. Ceram. Soc.*, 1988, **71**(10), 807–812.
17. Van Tendeloo, G., Faber, K. T. and Thomas, G., Characterization of AlN ceramics containing long-period polytypes. *J. Mater. Sci.*, 1983, **18**(2), 525–532.
18. Quinn, G. D., Corbin, N. D. and McCauley, J. W., Thermomechanical properties of aluminum oxynitride spinel. *Ceram. Bull.*, 1984, **63**(5), 723–729.
19. Slack, G. A., Tanzilli, R. A., Pohl, R. O. and Vandersande, J. W., The intrinsic thermal conductivity of AlN. *J. Phys. Chem. Solids.*, 1987, **48**(7), 641–647.
20. Enloe, J. H., Rice, R. W., Lau, J. W., Kumar, R. and Lee, S. Y., Microstructural effects on the thermal conductivity of polycrystalline aluminum nitride. *J. Am. Ceram. Soc.*, 1991, **74**(9), 2214–2219.
21. Horiguchi, A., Ueno, F., Kasori, M., Schinozaki, K. and Tsuge, A., Effect of sintering atmosphere on thermal conductivity and its microstructure for an AlN ceramic. In *Proc. 25th Symp. on the Basic Science of Ceramics;, Yogyo Kyokai* ID03, 1987, pp.155.
22. Virkar, A. V., Jackson, V. and Cutler, R. A., Thermodynamic and kinetic effects of oxygen removal on the thermal conductivity of aluminum nitride. *J. Am. Ceram. Soc.*, 1989, **72**(11), 2031–2042.
23. Buhr, H., Müller, G. and Wiggers, H., Phase composition, oxygen content, and thermal conductivity of AlN(Y_2O_3) ceramics. *J. Am. Ceram. Soc.*, 1991, **74**(4), 718–723.
24. Kim, W. J., Kim, D. K. and Kim, Ch.H., Morphological effect of second phase on the thermal conductivity of AlN ceramics. *J. Am. Ceram. Soc.*, 1996, **79**(4), 1066–1072.
25. Sternitzke, M. and Müller, G., EELS study of oxygen diffusion in aluminum nitride. *J. Am. Ceram. Soc.*, 1994, **77**(3), 737–742.
26. Jackson, T. B. and Virkar, A. V., High-thermal-conductivity aluminum nitride ceramics: the effect of thermodynamic, kinetic, and microstructural factors. *J. Am. Ceram. Soc.*, 1997, **80**(6), 1421–1435.
27. Corbin, N. D., State of the art aluminum oxynitride spinel: a review. *J. Eur. Ceram. Soc.*, 1989, **5**(1), 143–154.
28. Turpin-Launay, D., Goeuriot, P. and Thevenot, F., Nouveau matériau céramique composite contenant de l'alumine: l'aluminalon. *L'Industrie Ceram.*, 1983, **772**(5), 343–345.
29. Orange, G., Turpin-Launay, D., Goeuriot, P., Fantozzi, G. and Thevenot, F. Mechanical behaviour of a Al_2O_3–AlON composite ceramic material (Aluminalon). In *Science of Ceramics 12*. Ed. Vincenzini, 1983, pp. 661–666.
30. Ma, J., Liao, K. and Hing, P., Effect of aluminum nitride on properties of cordierite. *J. Mater. Sci.*, 2000, **35**(16), 4137–4141.
31. Fargas, G., Casellas, D., Llanes, L. and Anglada, M., Thermal shock resistance of yttria-stabilized zirconia with Palmqvist indentation cracks. *J. Eur. Ceram. Soc.*, 2003, **23**(1), 107–114.
32. Collin, M. and Rowcliffe, D., The morphology of thermal cracks in brittle materials. *J. Eur. Ceram. Soc.*, 2002, **22**, 435–445.
33. Osterstock, F., Monot, I., Desgardin, G. and Mordike, B. L., Influence of grain size on the toughness and thermal shock resistance of polycristalline $YBa_2Cu_3O_{7-\delta}$. *J. Eur. Ceram. Soc.*, 1996, **16**(7), 687–694.
34. Tancret, F. and Osterstock, F., The vickers indentation technique used to evaluate the thermal shock resistance of brittle materials. *Scripta Mater.*, 1997, **37**(4), 443–447.
35. Collin, M. and Rowcliffe, D., Analysis and prediction of thermal shock in brittle materials. *Acta Mater.*, 2000, **48**(8), 1655–1665.
36. Lee, S. K., Moretti, J. D. and Readey, M. J., Thermal shock resistance of silicon nitrides using an indentation-quench test. *J. Am. Ceram. Soc.*, 2002, **85**(1), 279–281.
37. Pettersson, P., Johnsson, M. and Shen, Z., Parameters for measuring the thermal shock of ceramic materials with an indentation-quench method. *J. Eur. Ceram. Soc.*, 2002, **22**(11), 1883–1889.
38. Anstis, G. R., Chantikul, P., Lawn, B. R. and Marshall, D. B., A critical evaluation of indentation techniques for measuring fracture toughness: I, direct crack measurements. *J. Am. Ceram. Soc.*, 1981, **64**(9), 533–538.
39. Lawn, B. and Wilshaw, R., Indentation fracture: principles and applications. *J. Mater. Sci.*, 1975, **10**, 1049–1081.
40. Marshall, V. and Lawn, B. R., Residual stress effects in sharp contact cracking. Part 1: indentation fracture principles. *J. Mater. Sci.*, 1979, **14**, 2001–2012.
41. Kingery, W. D., Bowen, H. K., Uhlmann, D. R. (eds), *Thermal and compositional stresses, Introduction to Ceramics*, 2nd ed. John Wiley & Sons, New York, USA, 1976, pp. 816–846.
42. Becher, P. F., Effect of water bath temperature on the thermal shock of Al_2O_3. *J. Am. Ceram. Soc.*, 1981, **64**(1), C–17-C-18.
43. Lynch, C. T., ed., *Handbook of Materials Science Vol. 1 General Properties*. CRC Press Inc, Cleveland, OH, 1974, pp. 366.
44. Miranzo, P. and Moya, J. S., Elastic-plastic indentation in ceramics: a fracture toughness determination method. *Ceramics International*, 1984, **10**(4), 147–152.
45. Kingery, W. D., Bowen, H. K., Uhlmann, D. R. (eds), *Thermal properties, Introduction to Ceramics*, 2nd ed. John Wiley & Sons, New York, USA, 1976, pp. 583–645.
46. Launay, D., Orange, G., Goeuriot, P., Thevenot, F. and Fantozzi, G., Reaction-sintering of an Al_2O_3–AlN composite determination of mechanical properties. *J. Mater. Sci. Letters*, 1984, **3**(10), 890–892.
47. Schlichting, K. W., Padture, N. P. and Klemens, P. G., Thermal conductivity of dense and porous ytria-stabilized zirconia. *J. Mater. Sci.*, 2001, **36**(12), 3003–3010.
48. Fett, T., An analysis of the residual stress intensity factor of Vickers indentation cracks. *Eng. Frac. Mec.*, 1995, **52**(4), 773–776.
49. Osterstock, F., Tancret, F., Vansse, O. and Kutschera, U., Quantification of quenching stresses and heat transfer. *Ann. Chim. Sci. Mat.*, 1998, **23**(1-2), 143–146.
50. Gong, J. H., Guan, Z. D. and Jiang, D. C., Analysis for strength degradation of indented specimens due to thermal shock. In *Fracture Mechanics of Ceramics, Vol.10*, ed. R. C. Bradt, D. P. H. Hasselman, D. Munz, M. Sakai and V.Ya. Shevchenko. Plenum Press, New York, 1992, pp. 605–610.
51. Sato, T., Fukushima, T., Endo, T. and Shimada, M., Thermal shock resistance of yttria-doped tetragonal zirconia polycrystals: effect solvent in quenching test. *J. Mater. Sci. Letters*, 1987, **6**(11), 1287–1290.